Tuning electron transfer by crystal facet engineering of $BiVO_4$ for boosting visible-light driven photocatalytic reduction of bromate

Liu, Guoshuai; Zhu, Yukun; Yan, Qun; Wang, Han; Wu, Peng; Shen, Yaoliang; Doekhi-Bennani, Yasmina

Important note
To cite this publication, please use the final published version (if applicable).
Please check the document version above.

Tuning electron transfer by crystal facet engineering of BiVO$_4$ for boosting visible-light driven photocatalytic reduction of bromate

Guoshuai Liu [a,1], Yukun Zhu [b,1], Qun Yan [a,c,*], Han Wang [a], Peng Wu [c], Yaoliang Shen [c], Yasmina Doekhi-Bennani [d]

[a] School of Environmental and Civil Engineering, Jiangnan University, Wuxi 214122, China
[b] School of Environmental Science and Engineering, State Key Laboratory of Bio-Fibers and Eco-Textiles, Qingdao University, Qingdao 266071, China
[c] Jiangsu Collaborative Innovation Center of Technology and Material of Water Treatment, Suzhou 215011, China
[d] Department of Water Management, Section Sanitary Engineering, Delft University of Technology, PO Box 5048, 2600, GA, Delft, the Netherlands

HIGHLIGHTS

- Monoclinic bismuth vanadate (BiVO$_4$) was obtained with the control of {010} and {110} facets.
- Photo-generated electrons and holes are transferred to {010} and {110} facets, respectively.
- BiVO$_4$ crystal photocatalyst with optimized {010} and {110} facets ratio exhibit highest bromate reduction efficiency.

GRAPHICAL ABSTRACT
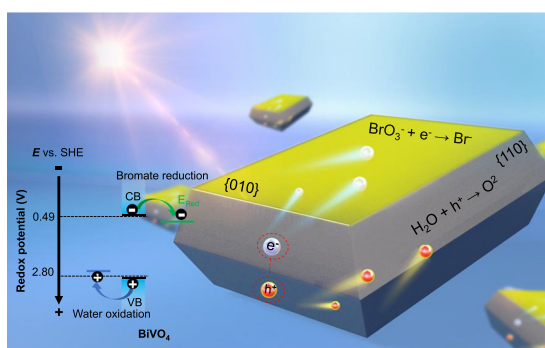
ARTICLE INFO

ABSTRACT

Removal of bromate (BrO$_3^-$) has gained increasing attention in drinking water treatment process. Photocatalysis technology is an effective strategy for bromate removal. During the photocatalytic reduction of bromate process, the photo-generated electrons are reductive species toward bromate reduction and photo-generated holes responsible for water oxidation. In this study, the monoclinic bismuth vanadate (BiVO$_4$) single crystal was developed as a visible photocatalyst for the effective removal of bromate. The as-synthesized BiVO$_4$ photocatalyst with optimized {010} and {110} facets ratio could achieve almost 100% removal efficiency of BrO$_3^-$ driven by visible light with a first-order kinetic constant of 0.0368 min^{-1}. As demonstrated by the electron scavenger experiment and density functional theory (DFT) calculations, the exposed facets of BiVO$_4$ should account for the high photocatalytic reduction efficiency. Under visible light illumination, the photo-generated electron and holes were spatially transferred to {010} facets and {110} facets, respectively. The BiVO$_4$ single crystal photocatalyst may serve as an attractive photocatalyst by virtue of its response to the visible light, spatially charge transfer and separation as well as high photocatalytic activity, which will make the removal of BrO$_3^-$ in water much easier, more economical and more sustainable.

© 2020 Elsevier B.V. All rights reserved.

1. Introduction

Bromate (BrO$_3^-$) originated from the chlorination or ozonation process in bromide-containing water has attracted the attention of many researchers (Bouland et al., 2005; Chen et al., 2016; Parker et al., 2014,

* Corresponding author at: School of Environmental and Civil Engineering, Jiangnan University, Wuxi 214122, China.
E-mail address: yanqun@jiangnan.edu.cn (Q. Yan).
[1] The authors contribute equally to this work.

Zhu et al., 2020b). The drinking water standard of BrO_3^- in the European Union and the U.S. Environmental Protection Agency is less than 10 μg L^{-1} (Shen et al., 2017; Weinberg et al., 2003; Wu et al., 2013). To overcome this obstacle, considerable progress has been made regarding the transformation of BrO_3^- to Br^- by using various technologies, such as electrochemical reductive treatment (Xie and Shang, 2007), zero-valent iron (Wang et al., 2009; Zhang et al., 2015) and FeOOH catalytic reduction (Nie et al., 2014). Although these already established technologies can remove BrO_3^- effectively, they may suffer from various problems such as high cost, operational complexity, as well as the potential secondary pollution risk induced by metal leaching (Ayoubi-Feiz et al., 2015; Lin et al., 2016; Noguchi et al., 2003).

Recently, photocatalysis process was regarded as a superior technology to remove BrO_3^- (Noguchi et al., 2002). Compared with the conventional removal methods mentioned above, photocatalysis shows fascinating potential for bromate removal systems due to its high efficiency, low-cost and environmental benignity (Ayoubi-Feiz et al., 2015; Lin et al., 2016; Noguchi et al., 2003). As the widely used photocatalyst, TiO_2 based photocatalysts had been extensively employed in bromate removal by UV-light driven photocatalysis, whereas the efficient conversion of BrO_3^- to Br^- was contributed to the photo-generated electrons at conduction band (CB) (Li et al., 2016; Liu et al., 2016; Zhang et al., 2005).

However, the photocatalytic systems based on TiO_2-photocatalysis still suffer from some problems for bromate removal: (i) The wide bandgap (E_g = 3.2 eV) of TiO_2 can only be responsively under UV light irradiation (UV, 3% ratio of solar light). This may cause inconvenience in practical applications (Perry Iv et al., 2009; Williams et al., 2008; Yang et al., 2020a; Yang et al., 2020b). (ii) The reducing agent in the photocatalytic system is photo-generated electrons. It is important to improve the quantum efficiency of photoelectrons to participate in the bromate reduction reaction (Pan and Zhu, 2010; Wang et al., 2020a; Yang et al., 2019; Zhu et al., 2020c; Wang et al., 2020b; Wang et al., 2019). (iii) As a redox couple in the reaction depends on generated-electrons and holes, the photocatalytic reduction half-reaction is interdependent to the oxidation half-reaction mediated by photo-generated holes at the valence band (VB). Therefore, there is a growing interest in developing high overall efficiency visible light driving photocatalysts (Zhang et al., 2019; Zhu et al., 2019; Zhu et al., 2020a).

In the BrO_3^- reduction system, BrO_3^- acts as an electron acceptor, and the reduction reaction (1 e^- process) is not considered as a limiting step for the overall photocatalytic redox reaction. On the other hand, the oxidation of water (4 e^- process) is observed as a bottleneck or the rate-determining step (Zhu et al., 2020b). Based on the above-mentioned points, the premise for effective BrO_3^- reduction is to find a visible photocatalyst with high reductive activity, high selectivity and water oxidation ability.

Monoclinic $BiVO_4$ has been widely used in photocatalysis or photoelectrochemical process for the water oxidation to produce oxygen due to its efficient and active visible light photocatalytic properties (Nakabayashi et al., 2017; Saison et al., 2015). Therefore, the oxidation reaction would not hamper the reductive half-reaction (bromate reduction reaction). On the premise that $BiVO_4$ can efficiently oxidize water, the major water oxidation products are oxygen rather than hydroxyl radicals (Nakabayashi et al., 2017; Saison et al., 2015). This can mitigate the problem of the re-oxidation of bromine ions by hydroxyl radicals. Recent associated studies on the preparation of single crystal $BiVO_4$ photocatalysts have shown that photo-generated carriers could be transferred to different exposed crystal facets (Li et al., 2013; Zhu et al., 2017), the reduction and oxidation reactions were spatially separated with a high reaction extent. Learned from these experiences, the reduction surface (photo-generated electron rich surface) of $BiVO_4$ can be made by the crystal facet engineering, thus improving the quantum efficiency of photo-generated electrons involved in the bromate reduction reaction.

Herein, three kinds of $BiVO_4$ crystals (BVO-a, b and c) with different exposed facets were prepared and applied to the photocatalytic reduction of bromate under visible light. Additionally, the structure and morphology of $BiVO_4$ single crystals were characterized using X-ray diffraction (XRD) and field emission scanning electron microscopy (FESEM). Furthermore, the BrO_3^- reduction performance was evaluated by calculating the conversion of BrO_3^- to Br^-. Lastly, the optical properties and electron configuration were estimated using density functional theory (DFT), and the bandgap, band position, and effective electron mass were also taken into consideration. The possible photocatalytic reduction mechanisms of BrO_3^- by $BiVO_4$ crystals were proposed.

2. Experimental section

2.1. Synthesis of the photocatalyst

$BiVO_4$ powders were prepared by liquid-solid state reaction. 5 mmol of V_2O_5 and 10 mmol of $Bi(NO_3)_3 \cdot 5H_2O$ were added in 60 mL of DI water. The precursor solution was stirred until a yellow solution was formed. The pH of the solution was regulated to 1.0, 0.5 and 0.1 by ammonia solution or dilute nitric acid solution, and then the solution was vigorously stirred at room temperature for 5 days. The obtained $BiVO_4$ powder was separated by centrifugation, washed with DI water and dried at 60 °C. Moreover, the obtained $BiVO_4$ powders synthesized at different pH values of 1.0, 0.5 and 0.1 were labeled as $BiVO_4$-a, $BiVO_4$-b and $BiVO_4$-c.

2.2. Characterization

The powder X-ray diffraction (XRD) characterization was conducted on an X-ray diffractometer (Bruker D8 Adv., Germany). The crystalline phase and morphology of the as-prepared $BiVO_4$ samples were characterized by an X-ray diffractometer (Bruker D8 Adv., Germany) and a field emission scanning electron microscope (FESEM, Type-4800, Hitachi, Japan), respectively. A spectrophotometer (Type-UV2550, Shimadzu, Japan) recorded the UV–vis diffuse reflectance spectroscopy (DRS) of the powders. The photoelectrochemical measurements were conducted using a CHI760E electrochemical workstation. The photocurrent measurements were carried out under visible light irradiation (300 W Xenon lamp).

2.3. Theoretical calculations

The optimization of the unit cell of monoclinic scheelite $BiVO_4$ was performed using the CASTEP code with the projector augmented wave (PAW) pseudopotentials (Liu et al., 2017), and the parameter was set according to the reference (Long et al., 2008). The angle b of monoclinic scheelite $BiVO_4$ was set to 134.9° for simplification, the detailed parameters can be found in Table S1. The stable crystal configuration of the bulk and the cleavage surface with the optimized lowest energy are shown in Fig. S1.

2.4. Experimental setup and procedures

The BrO_3^- ions removal performance was tested according to the previous method reported by our team (Liu et al., 2019). Both BrO_3^- and Br^- ions were determined by an ion chromatograph analyzer (LC-10A, Shimadzu, Japan).

3. Results and discussion

3.1. Characterization of $BiVO_4$ photocatalysts

The XRD patterns of three types of as-synthesized $BiVO_4$ photocatalysts are presented in Fig. 1A. All diffraction patterns of samples ($BiVO_4$-a, b and c) showed sharp diffraction peaks and all typical
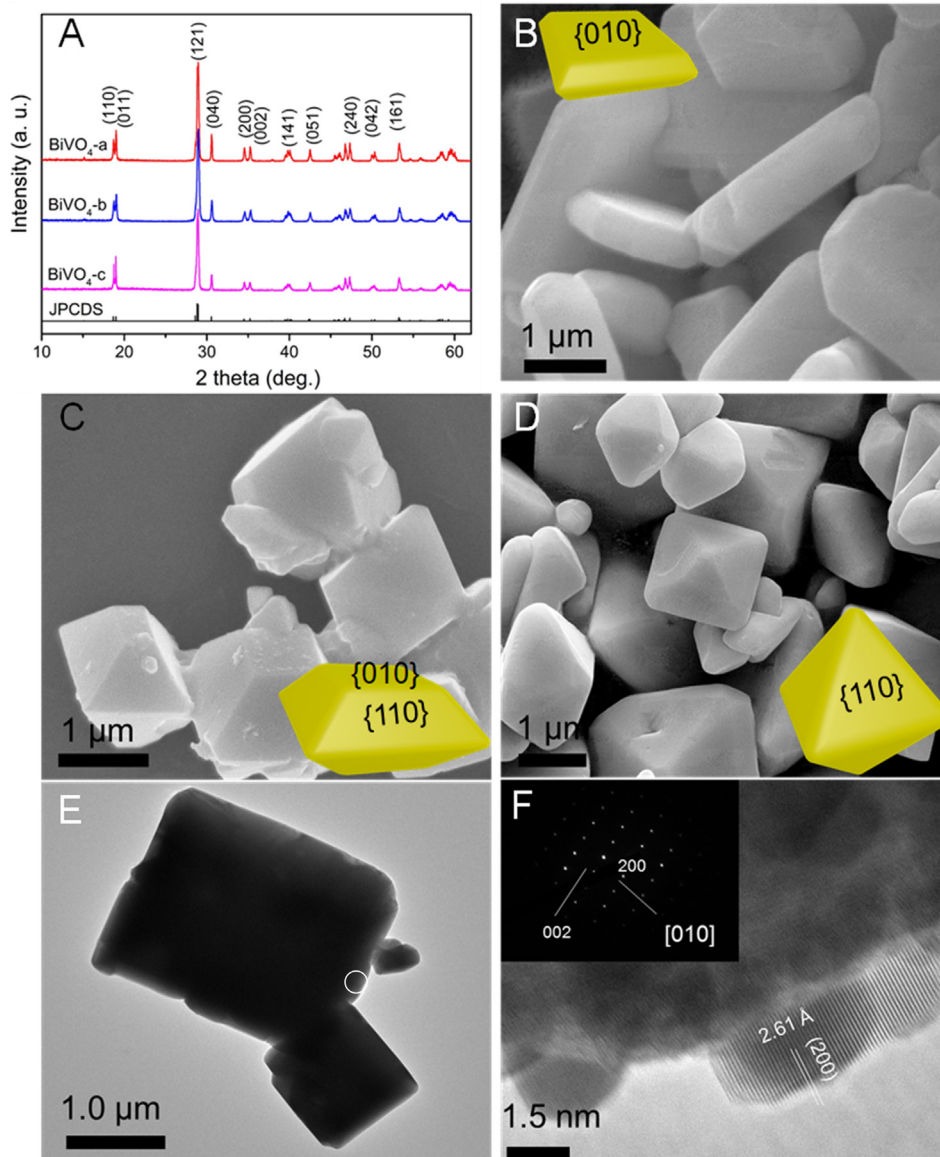
Fig. 1. XRD patterns of (A) BiVO$_4$ samples, SEM pictures of (B) BiVO$_4$-a, (C) BiVO$_4$-b, (D) BiVO$_4$-c, (E) TEM and HRTEM (F) pictures of BiVO$_4$-a.

peaks were attributed to monoclinic scheelite BiVO$_4$ crystal phase (JCPDS No. 14-0688, space group: $C2/c$), evidently suggesting that the BiVO$_4$ photocatalysts have high crystallinity (Liu et al., 2014). Considering the phenomenon that the (121) peak was the highest peak for separated BiVO$_4$-a, b and c, the (121) peak was selected as the benchmark to evaluate the possible exposed surface in BiVO$_4$ crystal qualitatively, i.e., the intensity ratios of the diffraction peak of (040) and (110) compared with (121). The intensity of (040) diffraction peak followed the order of BiVO$_4$-a > BiVO$_4$-b > BiVO$_4$-c, while that of (110) diffraction peak showed a reverse order, i.e., BiVO$_4$-c > BiVO$_4$-b > BiVO$_4$-a. However, the intensity of (110) diffraction peak of BiVO$_4$-c was stronger than that of BiVO$_4$-b and a (BiVO$_4$-c > BiVO$_4$-b > BiVO$_4$-a). According to Wang's study, this intensity difference in XRD pattern indicated that the (040) diffraction peak was the dominant peak for BiVO$_4$-a, and that for BiVO$_4$-c was (110) (Wang et al., 2011). The FESEM image of BiVO$_4$-a exhibited a sheet-like geometry with a length of 1.5 μm, width of 400-nm, and thickness of 150-nm, respectively (Fig. 1B). The BiVO$_4$-b sample exhibited a polyhedral box shape (Fig. 1C) with an average size of about 1.5 μm. In addition, the BiVO$_4$-c with an octahedral shape of about 2 μm was observed in

Fig. 1D. To further identify the exposed crystal faces, the corresponding HRTEM image for BiVO$_4$-a is given in Fig. 1E.

The corresponding selected area electron diffraction (SAED) pattern in Fig. 1F (inset picture) is taken from the sheet-like BiVO$_4$-a sample (Fig. 1E), revealing the growth orientation in accordance with the results of XRD measurements. As determined by XRD result, and with different b axis orientations for different sheets, the d spacings measured from SAED (zone axis [010]) were 2.61 Å, which agreed well with the lattice spacings of (200) monoclinic BiVO$_4$ (Wang et al., 2011). The growth direction was along the (040) facet, i.e., {010} crystal planes; therefore, the sheet-like BiVO$_4$-a grew along the b axis as seen in the HRTEM images (Fig. 1F). Based on these analyses and calculations, a simple schematic illustration of the exposed crystal surface is presented in the insets in Fig. 1B, C and D according to the XRD and HRTEM analysis. The XPS spectra of Bi 4f, V 2p and O 1s are illustrated in Fig. S2. The Bi 4f consisted of two peaks at the binding energy of 156.3 and 161.5 eV, while the V 2p spectra showed two peaks of 514.0 eV and 521.7 eV, respectively. Moreover, the O 1s spectra was detected at the binding energy of 527.1 eV.

3.2. Photocatalytic reduction of BrO_3^- by $BiVO_4$ photocatalysts

The feasibility of photocatalytic reduction of BrO_3^- using $BiVO_4$ photocatalysts under visible light irradiation were examined by photocatalytic experiment. No BrO_3^- reduction was observed in the absence of photocatalysts, which excluded the direct visible light driven photolysis of BrO_3^- reduction. As illustrated in Fig. 2A, the concentration of BrO_3^- decreased from initial 1000 to 0 μg L^{-1} (below the detection limit) for $BiVO_4$-b after 150 min of reaction, which exhibited almost 100% BrO_3^- removal efficiency. However, $BiVO_4$-a and $BiVO_4$-c reduced the initial BrO_3^- concentration (1000 μg L^{-1}) to 130 and 230 μg L^{-1}, respectively. The BrO_3^- removal performance can be well indexed to the first-order reaction $k = 0.0368$ min^{-1} for $BiVO_4$-b (Fig. 2B), which was 2.08 and 3.94 times higher than that of $BiVO_4$-a (0.0177 min^{-1}) and $BiVO_4$-c (0.0094 min^{-1}), respectively. (Table S2). These results demonstrated that the $BiVO_4$-b sample showed superior photocatalytic bromate removal performance than that of $BiVO_4$-a and -c samples which might be benefited from the facet effect of $BiVO_4$ crystal. Moreover, the stability of the $BiVO_4$ photocatalysts was also evaluated and the result can be seen in Fig. S3. during the recycling process, the photocatalytic performance of $BiVO_4$ was with high stability, amount to 3% activity loss after five-cycles. During the recycling process, the photocatalytic performance of $BiVO_4$ was of high stability with the activity loss amounting to 3% activity loss after five-cycles.

3.3. Mechanisms insight

To further understand the BrO_3^- reduction mechanism by $BiVO_4$ photocatalyst, the electron scavenger experiments were implemented by adding $S_2O_8^{2-}$ (Romão et al., 2015). As a typical electron scavenger, the degradation performance of BrO_3^- was decreased obviously after the introduction of $S_2O_8^{2-}$ (Fig. S4 and Table S3). Notably, the bromate removal nearly disappeared when 5 mmol of $K_2S_2O_8$ was added. Thus, it could be concluded that the photo-generated electrons were the reactive species during the BrO_3^- photocatalytic reduction process.

As we know, for semiconductor photocatalysis, the optical properties are directly related to the intrinsic electron configuration and thus influence the photocatalytic performance. Fig. 3A shows the DRS spectra of $BiVO_4$ samples with different exposed surfaces. The adsorption properties of the obtained three types of $BiVO_4$ were all typical visible light-driven photocatalysts with an absorption edge at approximately 536 nm ($E_g = 2.31$ eV), which was in line with the previous report (Su et al., 2011). The DFT calculation regarding optical properties was conducted to better understand the relationship of light absorption with exposed surface. As shown in Fig. 3B, there was no obvious difference in the absorption threshold for polycrystal, {010} and {110} facets

$BiVO_4$, respectively, which was in accordance with the DRS results. Based on the above DRS and DFT calculation results, it can be concluded that the optical properties of $BiVO_4$ samples may not be the major reasons for the great difference in the photocatalytic removal of bromate.

$$E_{VB} = \chi - E^e + \frac{E_g}{2} \tag{1}$$

$$E_{CB} = E_{VB} - E_g \tag{2}$$

Furthermore, the theoretical positions of energy band position of $BiVO_4$ at pH = pH$_{pzc}$ were calculated using the following conventional Eqs. (1) and (2) (Xu and Schoonen, 2000). E_e is the free electron energy (4.5 V), E_g is the measured band gap. By substituting these absolute electronegativities of Bi, V and O to Eq. (1) and (2), the E_{VB} of 2.80 V and E_{CB} of 0.49 V (SHE) were obtained (Cooper et al., 2014). Although the valence band position of $BiVO_4$ was suitable for hydroxyl radicals generation, according to the previous literature, $BiVO_4$ was generally considered as a highly efficient photocatalyst for water oxidation to produce oxygen rather than hydroxyl radicals, thus making the reduction of BrO_3^- more efficient toward Br$^-$ conversion (Nakabayashi et al., 2017; Saison et al., 2015).

As shown in Fig. S1, VO_4^{3-} was a stretched tetrahedron. In the stretched BiO_8 dodecahedron, Bi atoms were surrounded by 8 O atoms, and the four bond lengths were different (2.467, 2.466, 2.471, and 2.528 Å) (Stoltzfus et al., 2007; Yang et al., 2013). As we know, the dipole moments played an important role in photocatalysis, especially on the effective separation of carriers. A big dipole moment always means a high driving force makes efficient photo-generated carriers transfer (Li et al., 2014). In this regard, the absolute numerical value of dipole moment is calculated to be 0.79 and 0.68 D on {010} and {110} facets, respectively. The larger dipole moment of the BiO polyhedrons for {010} facet demonstrates greater distortion of the {110} surface layer, hence leading to a larger internal polarization which is conducive to the charge separation and higher activity for the photocatalytic reduction of BrO_3^-.

To further understand the electronic configuration of the two exposed crystal facets, the band structure of $BiVO_4$ is plotted in Fig. 4A. Considering the symmetry of the monoclinic system, the path selected from the Brillouin zone was along Z → G → Y → A → B → D → E → C. The DFT calculated E_g for $BiVO_4$ was 2.12 eV, close to the experimental value (2.31 eV). The highest band energy level and lowest energy level were located at different K-points, which indicated the typical indirect band gap property. Furthermore, we can calculate the effective carrier masses of {010} and {110} facets based on the curvatures of the bands in the corresponding directions by fitting parabolic functions to the conduction band minimum (CBM) and valence band maximum
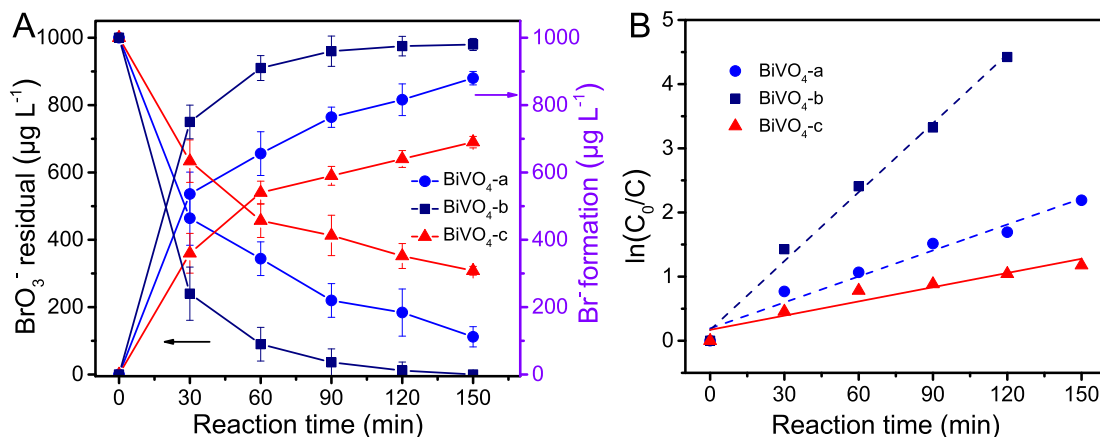

Fig. 2. Time course of (A) photocatalytic reduction of BrO_3^- by $BiVO_4$ photocatalysts under visible light irradiation at pH 7.1 ± 0.4, (B) the corresponding kinetics rate constants derived from A.
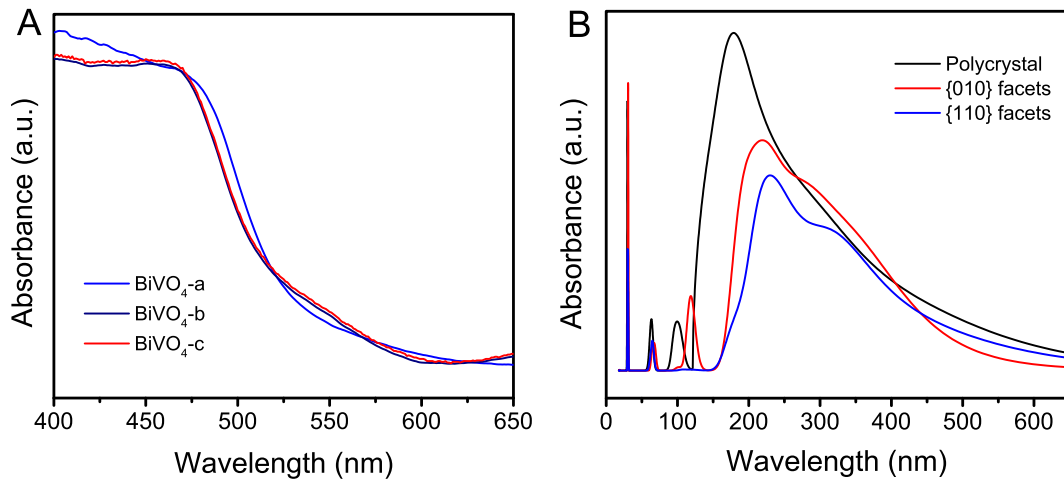
Fig. 3. (A) The experimental diffuse reflectance spectra of BiVO$_4$ samples, (B) calculated absorption coefficient of polycrstal BiVO$_4$, {010} and {110} facets exposed BiVO$_4$.
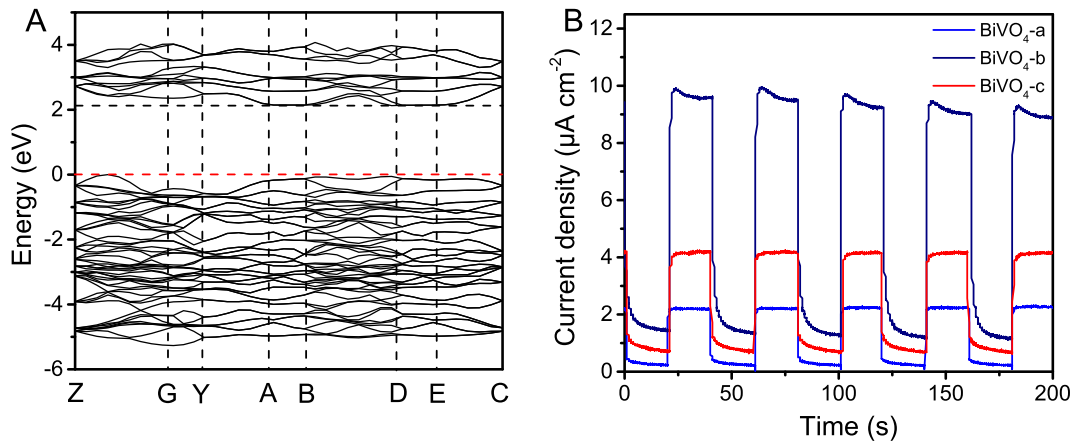

Fig. 4. The band structure (A) of BiVO$_4$ crystal and (B) photocurrent-time curve of BiVO$_4$ samples.

(VBM) of BiVO$_4$. According to the Eq. (3) (Li et al., 2014), the effective electron masses can be estimated, where k is the wave vector, and E_k is the energy corresponding to the wave vector k.

$$m^* = \pm h^2 \left(\frac{d^2 E_k}{dk^2} \right)^{-1} \qquad (3)$$

The calculated results are summarized in Table 1. The effective electron masses were approximately 0.13 m$_0$ and 0.30 m$_0$, and the effective hole masses are estimated to be approximately 0.18 m$_0$ and 0.57 m$_0$ for {010} and {110} surfaces, respectively. In the photocatalytic process, lower effective mass means higher drift velocity, and the photo-generated hole/electron pairs could be transferred to the surface of photocatalyst (Li et al., 2014). Therefore, the effective electron mass of {010} was 0.13 m$_0$, obviously lower than that of {110} facets making it favorable for the photocatalytic bromate reduction process.

Table 1
Summary of the effective masses.

	{010}/m$_0$	{110}/m$_0$
m_h^*	0.18	0.57
m_e^*	0.13	0.30

According to the dipole moment and charge transport calculation, the presence of {010} facet exposed BiVO$_4$ was beneficial for the charge separation. As revealed from the photocurrent of BiVO$_4$-a, BiVO$_4$-b and BiVO$_4$-c in Fig. 4B, BiVO$_4$-b possessed a much higher photocurrent than BiVO$_4$-a and BiVO$_4$-c. The intense photocurrent generally means a higher hole/electron pairs separation efficiency (Li et al., 2017). As shown in Fig. 4B, the BiVO$_4$-b sample with {010} facet exposed maintained a high separation efficiency of hole/electron pairs, which was in well agreement with the result of dipole moment calculations.

The intrinsic reason for the separation of photo-generated carriers on the {010} and {110} of BiVO$_4$ crystal facets was evaluated by the DFT calculation method (Pan et al., 2011). Fig. 5A shows the density of states (DOS) calculation results (where Fermi energy was set as 0 eV). We can ascertain the conduction band edge and valence band edge from Fig. 5A, where the conduction band edge for {110} facets was 1.33 eV, and that for {010} was 2.15 eV. Thus, the energy differences for conduction bands (Δ_{CB}) between {010} and {110} facets was about 0.82 eV. Similarly, we could calculate the Δ_{VB} by analyzing the DOS curves and the result is about 0.20 eV between {010} and {110} facets. The existed difference well demonstrated that the transfer trend of photo-generated electron was from {110} to {010} facets in the thermo-dynamic view. Within this context, the electrons were accumulated on {010} facets, whereas the holes were enriched on {110} facets. Based on the calculated results obtained in Fig. 5A, the schematic diagram of spatial photo-generated carriers separation between {110} and {010} facets
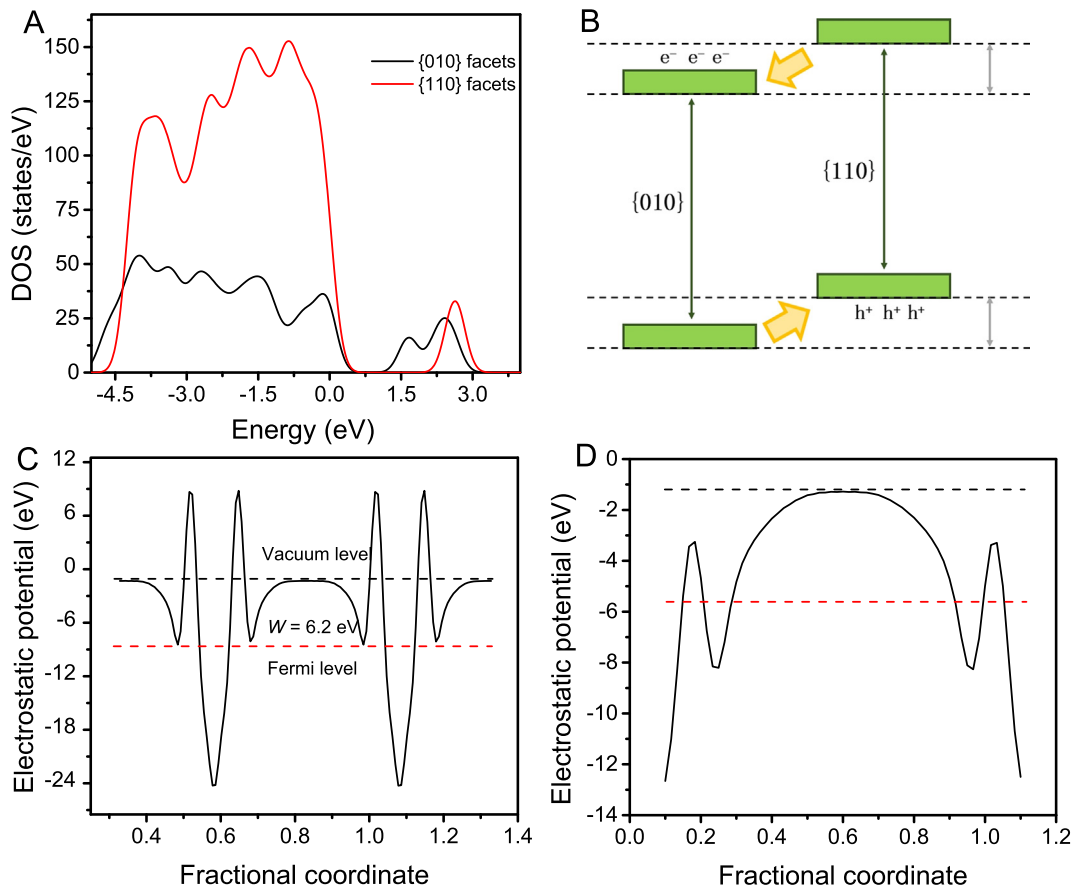
Fig. 5. (A) The differences of the energy levels in conduction bands (Δ_{CB}) for {010} and {110} facets, (B) the scheme of carrier separation between {010} and {110} facets, (C) the workfunction (W) of {010} surface and (D) {110} surface.

is schematic shown in Fig. 5B. Furthermore, the Work function (W) calculation results are shown in Fig. 5C and D. The W of {010} and {110} facets was 6.2 eV and 4.5 eV, respectively. The W value of {010} facets is obvious bigger than that of {110} facets, which makes the {010} facets have a higher electron capture ability (Gao et al., 2011). The results were in line with the density of state (DOS) analysis, where the photo-generated electrons were separated spatially with the photo-generated holes during photocatalytic process to form electron-rich {010} facets and hole-rich {110} facets.

For a practical photocatalytic reaction, reduction reactions were accompanied by oxidation reactions. To achieve a high photocatalytic efficiency (in this study, is photocatalytic reduction of bromate), high oxidation reactions involved by photo-generated holes must be considered. To clarify the mechanism deeply, the test of BiVO$_4$ photocatalyst utilized in water oxidation under visible light irradiation of O$_2$ evolution with BrO$_3^-$ as electron sacrificial agent (NaBrO$_3$, 0.1 mol L^{-1}) was conducted, and the photocatalytic O$_2$ evolution performance is shown in Table S4. As shown in Table S4, the BiVO$_4$-b exhibited the highest oxygen production with the rate of 11.70 μmol h^{-1}, and the order of oxygen production rate was BiVO$_4$-b (11.70 μmol h^{-1}) ≫ BiVO$_4$-a (2.30 μmol h^{-1}) > BiVO$_4$-c (1.50 μmol h^{-1}). The results evidently confirmed that the BiVO$_4$-b showed the highest water oxidation, as an overall reaction, the photo-reduction performance was correlated with the oxidation ability. Therefore, the BiVO$_4$-b sample with an optimized exposure ratio of the {010} and {110} surfaces exhibited the highest photocatalytic bromate reduction activity. The conceivable intrinsic mechanisms are schematically showed in Fig. 6. Under the irradiation of visible light, photo-generated carriers were separated toward different surfaces for the polyhedral box shape BiVO$_4$ photocatalyst, i.e., the photo-generated electrons (thermodynamic potential of 0.49 V, SHE)

and photo-generated holes (2.80 V, SHE) were transferred to different facets of BiVO$_4$ crystal. As shown in Fig. 6, the {010} facets were the electron-rich surfaces, whereas the holes were accumulated on the {110} surfaces. The electron with a redox potential of 0.49 V was a robust reductive for bromate reduction (BrO$_3^-$ + 6H$^+$ + 6e$^-$ → Br$^-$ + 3H$_2$O, $E^\ominus = 1.423$ V). And photo-generated hole with a high redox potential of 2.80 V could decompose H$_2$O to produce oxygen efficiently (2H$_2$O − 4e$^-$ → O$_2$ + 4H$^+$, $E^\ominus = 1.23$ V). In this manner, BrO$_3^-$ could be regarded as the electron acceptor and in-situ reduced at {010} facets, while the water oxidation reaction was occurred at {110} surfaces to produce O$_2$. The photo-generated electron-hole pairs were spatially separated, and the oxidation and reduction reactions occurred at different crystal
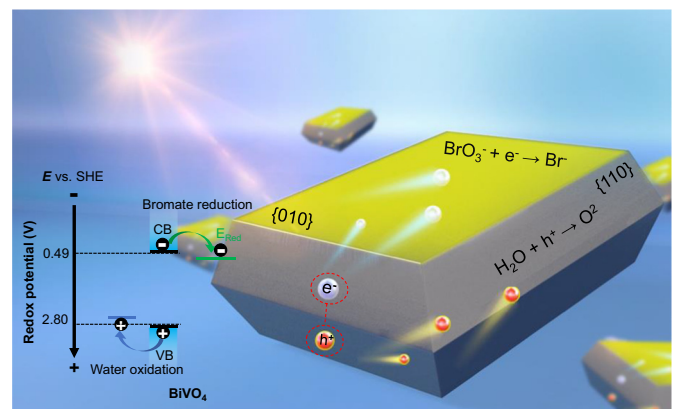

Fig. 6. Schematic illustration of photocatalytic reduction of BrO$_3^-$ by BiVO$_4$-b.

facets; thus, a high bromate reduction efficiency and selectivity on $BiVO_4$ single crystal with optimized {010} and {110} ratio could be achieved. Besides, a systemic comparison with conventional photocatalyst of TiO_2, traditional bulk $BiVO_4$ or Bi_2MoO_6 documented from literature is summarized in Table S5. The $BiVO_4$-b sample with active exposed facets ratio could remove almost 100% of BrO_3^-, whose kinetic constant was significantly higher than that of other conventional photocatalysts.

4. Conclusions

To achieve efficient removal of BrO_3^-, we herein developed single crystal photocatalysts $BiVO_4$ with different exposed facets. The {010} facets are exposed electron-rich surfaces with a higher dipole moment and a lower effective masse of electrons/holes, which is more favorable for the photocatalytic bromate reduction reaction. Under visible light illumination, the photo-generated reductive electrons and oxidative photo-generated holes are spatially transported to {010} and {110} facets, respectively. During the bromate photocatalytic removal process, water acts as an electron donor, thus avoiding the risk of secondary pollution, making the BrO_3^- removal of high efficiency. This investigation provides a simple and effective strategy for enhanced degradation of bromate without complicated preparation procedure, which makes the bromate removal more efficient and sustainable, and also gives a guideline for the development of single crystal photocatalyst for bromate photocatalytic reduction.

CRediT authorship contribution statement

Guoshuai Liu: Writing-Original Draft.
Yukun Zhu: Validation, Formal analysis.
Qun Yan: Resources, Supervision.
Han Wang: Language-Review & Editing.
Peng Wu: Resources.
Yaoliang Shen: Resources and Editing.
Yasmina Doekhi-Bennani: Writing: Review & Editing.

Declaration of competing interest

We declare that we have no financial and personal relationships with other people or organizations that can inappropriately influence our work, there is no professional or other personal interest of any nature or kind in any product, service and/or company that could be construed as influencing the position presented in, or the review of, the manuscript entitled "Tuning Electron Transfer by Crystal Facet Engineering of $BiVO_4$ for Boosting Visible-Light Driven Photocatalytic Reduction of Bromate".

Acknowledgements

Appendix A. Supplementary data

Supplementary data to this article can be found online at https://doi.org/10.1016/j.scitotenv.2020.143086.

References

Bouland, S., Duguet, J.-P., Montiel, A., 2005. Evaluation of bromate ions level introduced by sodium hypochlorite during post-disinfection of drinking water. Environ. Technol. 26, 121–126.

Chen, F., Yang, Q., Zhong, Y., An, H., Zhao, J., Xie, T., et al., 2016. Photo-reduction of bromate in drinking water by metallic Ag and reduced graphene oxide (RGO) jointly modified $BiVO_4$ under visible light irradiation. Water Res. 101, 555–563.

Cooper, J.K., Gul, S., Toma, F.M., Le, C., Glans, P.A., Guo, J., et al., 2014. Electronic structure of monoclinic $BiVO_4$. Chem. Mater. 26, 5365–5373.

Gao, E., Wang, W., Shang, M., Xu, J., 2011. Synthesis and enhanced photocatalytic performance of graphene-Bi_2WO_6 composite. Phys. Chem. Chem. Phys. 13, 2887–2893.

Li, R., Zhang, F., Wang, D., Yang, J., Li, M., Zhu, J., et al., 2013. Spatial separation of photogenerated electrons and holes among {010} and {110} crystal facets of $BiVO_4$. Nat. Commun. 4, 1432–1439.

Li, Z., Dai, Y., Ma, X., Zhu, Y., Baibiao, H., 2014. Tuning photocatalytic performance of the near-infrared-driven photocatalyst $Cu_2(OH)PO_4$ based on effective mass and dipole moment. Phys. Chem. Chem. Phys. 16, 3267–3273.

Li, X., Pi, Y., Xia, Q., Li, Z., Xiao, J., 2016. TiO_2 encapsulated in Salicylaldehyde-NH_2-MIL-101 (Cr) for enhanced visible light-driven photodegradation of MB. Appl. Catal. B-Environ. 191, 192–201.

Li, Y., Jiang, Y., Ruan, Z., Lin, K., Yu, Z., Zheng, Z., et al., 2017. Simulation-guided synthesis of graphitic carbon nitride beads with 3D interconnected and continuous meso/macropore channels for enhanced light absorption and photo-catalytic performance. J. Mater. Chem. A 5, 21300–21312.

Lin, K.-Y.A., Lin, C.-H., Chen, S.-Y., Yang, H., 2016. Enhanced photocatalytic reduction of concentrated bromate in the presence of alcohols. Chem. Eng. J. 303, 596–603.

Liu, G., Liu, S., Lu, Q., Sun, H., Xu, F., Zhao, G., 2014. Synthesis of monoclinic $BiVO_4$ microribbons by sol-gel combined with electrospinning process and photocatalytic degradation performances. J. Sol-Gel Sci. Techn. 70, 24–32.

Liu, G., You, S., Ma, M., Huang, H., Ren, N., 2016. Removal of nitrate by photocatalytic denitrification using nonlinear optical material. Environ. Sci. Technol. 50, 11218–11225.

Liu, G., You, S., Tan, Y., Ren, N., 2017. In situ photochemical activation of sulfate for enhanced degradation of organic pollutants in water. Environ. Sci. Technol. 51, 2339–2346.

Liu, G., You, S., Zhang, Y., Huang, H., Spanjers, H., 2019. Conjugated donor-acceptor (D-A) supramolecule catalyst for visible-light-driven photocatalytic removal of bromate in water. J. Colloid Interf. Sci. 553, 666–673.

Long, M., Cai, W., Kisch, H., 2008. Visible light induced photoelectrochemical properties of n-$BiVO_4$ and n-$BiVO_4$/p-Co_3O_4. J. Phys. Chem. C 112, 548–554.

Nakabayashi, Y., Nishikawa, M., Saito, N., Terashima, C., Fujishima, A., 2017. Significance of hydroxyl radical in photoinduced oxygen evolution in water on monoclinic bismuth vanadate. J. Phys. Chem. C 121, 25624–25631.

Nie, Y., Hu, C., Li, N., Yang, L., Qu, J., 2014. Inhibition of bromate formation by surface reduction in catalytic ozonation of organic pollutants over β-FeOOH/Al_2O_3. Appl. Catal. B-Environ. 147, 287–292.

Noguchi, H., Nakajima, A., Watanabe, T., Hashimoto, K., 2002. Removal of bromate ion from water using TiO_2 and alumina-loaded TiO_2 photocatalysts. Water Sci. Technol. 46, 27–31.

Noguchi, H., Nakajima, A., Watanabe, T., Hashimoto, K., 2003. Design of a photocatalyst for bromate decomposition: surface modification of TiO_2 by pseudo-boehmite. Environ. Sci. Technol. 37, 153–157.

Pan, C., Zhu, Y., 2010. New type of $BiPO_4$ oxy-acid salt photocatalyst with high photocatalytic activity on degradation of dye. Environ. Sci. Technol. 44, 5570–5574.

Pan, J., Liu, G., Lu, G.Q., Cheng, H.M., 2011. On the true photoreactivity order of {001}, {010}, and {101} facets of anatase TiO_2 crystals. Angew. Chem. Int. Edit. 50, 2133.

Parker, K.M., Zeng, T., Harkness, J., Vengosh, A., Mitch, W.A., 2014. Enhanced formation of disinfection byproducts in shale gas wastewater-impacted drinking water supplies. Environ. Sci. Technol. 48, 11161–11169.

Perry Iv, J.J., Perman, J.A., Zaworotko, M.J., 2009. Design and synthesis of metal–organic frameworks using metal–organic polyhedra as supermolecular building blocks. Chem. Soc. Rev. 38, 1400–1417.

Romão, J.S., Hamdy, M.S., Mul, G., Baltrusaitis, J., 2015. Photocatalytic decomposition of cortisone acetate in aqueous solution. J. Hazard. Mater. 282, 208–215.

Saison, T., Chemin, N., Chanéac, C., Durupthy, O., Mariey, L., Fo, Maugé, et al., 2015. New insights into $BiVO_4$ properties as visible light photocatalyst. J. Phys. Chem. C 119, 12967–12977.

Shen, W., Lin, F., Jiang, X., Li, H., Ai, Z., Zhang, L., 2017. Efficient removal of bromate with core-shell Fe@Fe_2O_3 nanowires. Chem. Eng. J. 308, 880–888.

Stoltzfus, M.W., Woodward, P.M., Ram, S., Jae-Hyun, K., Bruce, B., 2007. Structure and bonding in $SnWO_4$, $PbWO_4$, and $BiVO_4$: lone pairs vs inert pairs. Inorg. Chem. 46, 3839–3850.

Su, J., Guo, L., Bao, N., Grimes, C.A., 2011. Nanostructured WO_3/$BiVO_4$ Heterojunction films for efficient photoelectrochemical water splitting. Nano Lett. 11, 1928–1933.

Wang, Q., Snyder, S., Kim, J., Choi, H., 2009. Aqueous ethanol modified nanoscale zerovalent iron in bromate reduction: synthesis, characterization, and reactivity. Environ. Sci. Technol. 43, 3292–3299.

Wang, D., Jiang, H., Zong, X., Xu, Q., Ma, Y., Li, G., et al., 2011. Crystal facet dependence of water oxidation on $BiVO_4$ sheets under visible light irradiation. Chem. Eur. J. 17, 1275–1282.

Wang, W., Han, Q., Zhu, Z., Zhang, L., Zhong, S., Liu, B., 2019. Enhanced photocatalytic degradation performance of organic contaminants by heterojunction photocatalyst $BiVO_4$/TiO_2/RGO and its compatibility on four different tetracycline antibiotics. Adv. Powder Technol. 30, 1882–1896.

Wang, Y., Ding, K., Xu, R., Yu, D., Wang, W., Gao, P., et al., 2020a. Fabrication of $BiVO_4$/$BiPO_4$/GO composite photocatalytic material for the visible light-driven degradation. J. Clean. Prod. 247, 119108.

Ayoubi-Feiz, B., Aber, S., Sheydaei, M., 2015. Effect of oxidants on photoelectrocatalytic decolourization using α-Fe_2O_3/TiO_2/activated charcoal plate nanocomposite under visible light. RSC Adv. 5, 19368–19378.

Wang, Y., Yu, D., Wang, W., Gao, P., Zhong, S., Zhang, L., et al., 2020b. Synthesizing Co₃O₄-BiVO₄/g-C₃N₄ heterojunction composites for superior photocatalytic redox activity. Sep. Purif. Technol. 239, 116562.

Weinberg, H.S., Delcomyn, C.A., Unnam, V., 2003. Bromate in chlorinated drinking waters: occurrence and implications for future regulation. Environ. Sci. Technol 37, 3104–3110.

Williams, G., Seger, B., Kamat, P.V., 2008. TiO₂-graphene nanocomposites. UV-assisted photocatalytic reduction of graphene oxide. ACS Nano 2, 1487–1491.

Wu, X., Yang, Q., Xu, D., Zhong, Y., Luo, K., Li, X., et al., 2013. Simultaneous adsorption/reduction of bromate by nanoscale zerovalent iron supported on modified activated carbon. Ind. Eng. Chem. Res. 52, 12574–12581.

Xie, L., Shang, C., 2007. The effects of operational parameters and common anions on the reactivity of zero-valent iron in bromate reduction. Chemosphere 66, 1652–1659.

Xu, Y., Schoonen, M.A.A., 2000. The absolute energy position of conduction and valence bands of selected semiconducting minerals. Am. Mineral. 85, 543–556.

Yang, J., Wang, D., Zhou, X., Li, C., 2013. A theoretical study on the mechanism of photocatalytic oxygen evolution on BiVO₄ in aqueous solution. Chem. Eur. J. 19, 1320–1326.

Yang, R., Dong, F., You, X., Liu, M., Zhong, S., Zhang, L., et al., 2019. Facile synthesis and characterization of interface charge transfer heterojunction of Bi₂MoO₆ modified by Ag/AgCl photosensitive material with enhanced photocatalytic activity. Mater. Lett. 252, 272–276.

Yang, R., Zhong, S., Zhang, L., Liu, B., 2020a. PW12/CN@ Bi₂WO₆ composite photocatalyst prepared based on organic-inorganic hybrid system for removing pollutants in water. Sep. Purif. Technol. 235, 116270.

Yang, R., Zhu, Z., Hu, C., Zhong, S., Zhang, L., Liu, B., et al., 2020b. One-step preparation (3D/2D/2D) BiVO₄/FeVO₄@rGO heterojunction composite photocatalyst for the removal of tetracycline and hexavalent chromium ions in water. Chem. Eng. J. 390, 124522.

Zhang, F., Jin, R., Chen, J., Shao, C., Gao, W., Li, L., et al., 2005. High photocatalytic activity and selectivity for nitrogen in nitrate reduction on Ag/TiO₂ catalyst with fine silver clusters. J. Catal. 232, 424–431.

Zhang, Y., Jing, S., Liu, H., 2015. Reactivity and mechanism of bromate reduction from aqueous solution using Zn–Fe(II)–Al layered double hydroxides. Chem. Eng. J. 266, 21–27.

Zhang, H., Yu, D., Wang, W., Gao, P., Zhang, L., Zhong, S., et al., 2019. Construction of a novel BON-Br-AgBr heterojunction photocatalysts as a direct Z-scheme system for efficient visible photocatalytic activity. Appl. Surf. Sci. 497, 143820.

Zhu, J., Pang, S., Dittrich, T., Gao, Y., Nie, W., Cui, J., et al., 2017. Visualizing the nano cocatalyst aligned electric fields on single photocatalyst particles. Nano Lett. 17, 6735–6741.

Zhu, Y., Li, J., Dong, C., Ren, J., Huang, Y., Zhao, D., et al., 2019. Red phosphorus decorated and doped TiO₂ nanofibers for efficient photocatalytic hydrogen evolution from pure water. Appl. Catal. B-Environ. 255, 117764.

Zhu, Y., Lv, C., Yin, Z., Ren, J., Yang, D., 2020a. A [001]-oriented hittorf's phosphorus nanorods/polymeric carbon nitride heterostructure for boosting wide-spectrum-responsive photocatalytic hydrogen evolution from pure water. Angew. Chem. Int. Edi. 59, 868–873.

Zhu, Y., Ren, J., Zhang, X., Yang, D., 2020b. Elemental red phosphorus-based materials for photocatalytic water purification and hydrogen production. Nanoscale 12, 13297–13310.

Zhu, Z., Wang, C., Liang, L., Yu, D., Sun, J., Zhang, L., et al., 2020c. Synthesis of novel ternary photocatalyst Ag₃PO₄/Bi₂WO₆/multi-walled carbon nanotubes and its enhanced visible-light photoactivity for photodegradation of norfloxacin. J. Nanosci. Nano. 20, 2247–2258.